Single cell and spatial multiomics identifies Alzheimer's disease markers

Abstract

The pathogenesis of Alzheimer's disease (AD) is incompletely understood. Single cell and spatial solutions are powerful tools to improve our understanding of disease development and progression by offering insights into how chromatin accessibility and gene expression, specific to cell type and spatial localization, are associated with neuropathology. Here, we used a multiomics approach, combining Chromium Single Cell Multiome ATAC + Gene Expression and Visium Spatial Gene Expression for FFPE plus immunofluorescence protein detection, to resolve the relationship between progressive changes in cell type–specific differential gene expression and plaque burden in the TgCRND8 AD-like mouse model. We identified differences in gene expression and chromatin accessibility of well-known AD markers between transgenic and wild-type (WT) mice in concordance with plaque burden. We also uncovered the spatial organization of these changes across anatomical brain regions.

Highlights

- Several AD-related markers showed differential expression between transgenic and WT mice in microglia and oligodendrocytes at different time points
- Motif enrichment analysis of differentially accessible chromatin regions identified transcription factors (TFs) involved with amyloid plaque deposition
- Spatial analysis showed localized gene expression changes occurring in discrete anatomical brain regions
- Multiomic data analysis yielded new insights into single cell, chromatin, and spatial gene expression differences throughout the course of disease progression in an AD-like mouse model

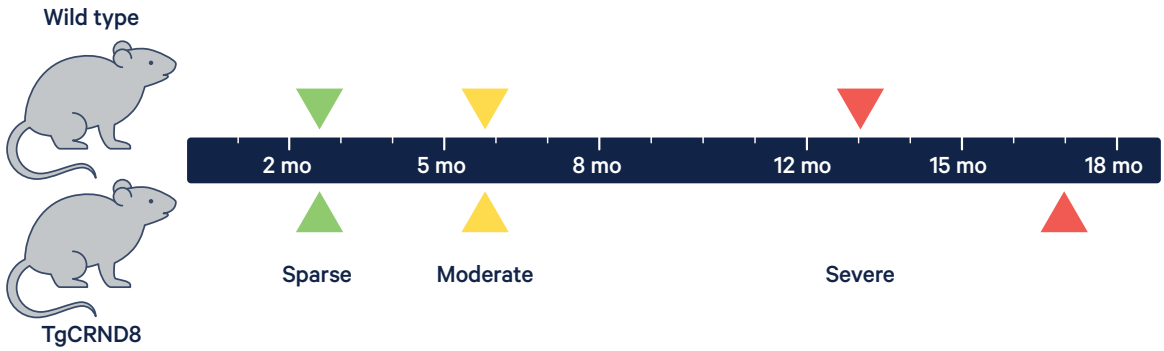

Figure 1. Experimental design. Twelve mouse brains were collected at timepoints spanning early, middle, and late life. Two replicates were collected per timepoint from TgCRND8 mice (n = 6) and WT littermates (n = 6). Selected timepoints were 2.5, 5.7, and 13.2 months of age for WT mice, and 2.5, 5.7, and 17.9 months of age for transgenic line. In TgCRND8 mice, plaque burden was sparse at 2.5 months, moderate at 5.7 months, and severe at 17.9 months, consistent with previous studies (3).

Introduction

Numerous studies have used single cell transcriptomic profiling to characterize gene expression differences in discrete cell types in AD, but fewer studies have combined that analysis with assessment of transcriptional regulation and spatially localized cell-type changes to more completely understand disease pathogenesis and progression. Studies using single cell chromatin accessibility profiling have begun to define the regulatory landscape of AD, underscoring the role of non-neuronal cells in the pathology of the disease (1). Recently, one study took a spatial approach to characterize gene expression networks around plaque deposits (2). Despite these advances, a cohesive demonstration of how gene expression is regulated within discrete cell types and specific anatomical regions of the brain during the early stages of AD is still unavailable, though it is crucial to identifying novel therapeutic targets.

To gain a holistic view of cell type–specific contributions to pathogenesis, map anatomical protein accumulation in the brain over time, and understand the relationship between abnormal protein accumulation and cellular phenotypes, we utilized a multiomics approach. Using Chromium Single Cell Multiome ATAC (Assay for Transposase-Accessible Chromatin) + Gene Expression (the multiome assay), which profiles open chromatin and gene expression from the same cell, and Visium Spatial Gene Expression for FFPE (Visium for FFPE) plus immunofluorescence (IF), which combines whole transcriptome spatial analysis with immunofluorescence protein detection in the same tissue section, we evaluated the open chromatin landscape and gene expression profiles in brains of TgCRND8 transgenic AD-like mice (3) and WT mice ranging from 2 to 13+ months old (early- to late-stage plaque deposition).

In this Application Note, we demonstrate how a multiomic approach provides a more complete assessment for furthering our understanding of mechanisms of disease pathogenesis. Integrating data from single cell gene expression, chromatin state, spatial transcriptomics, and IF protein detection, we analyzed amyloid beta (Aβ)-associated neuroinflammation across several anatomical regions of the brain and correlated these data with regulatory programs identified based on single cell multiomic and spatial transcriptomic data. We confirm the predicted spatial distribution of plaque burden over the course of pathology progression, identify specific neuroinflammatory markers differentially expressed with increasing amyloid accumulation and observed in discrete cell types, and localize these cells to specific brain regions.

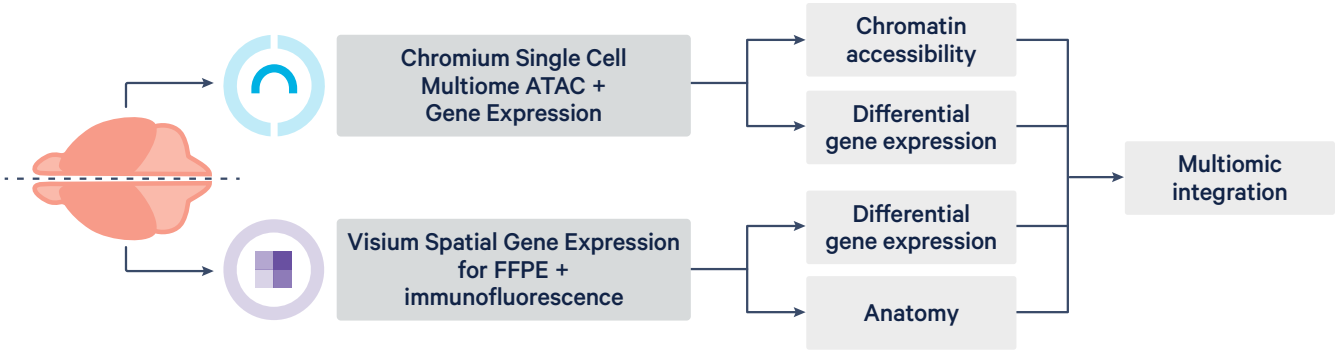

Figure 2. Multiomic integration from a single mouse brain. Each brain was divided by hemisphere, resulting in 24 separate samples for each timepoint. One hemisphere was flash frozen and used in the multiome assay. The other hemisphere was formalin-fixed, paraffin-embedded and used in the Visium for FFPE assay. These complementary data types were ultimately integrated in downstream analyses (Seurat and Signac).

Methods

Sample procurement and preparation. We analyzed 12 brains from male TgCRND8 mice (n = 6) and WT littermates (n = 6). For each genotype, two replicates at three different timepoints were analyzed (Figure 1). Selected timepoints were 2.5, 5.7, and 13.2 months of age for the WT mice, and 2.5, 5.7, and 17.9 months of age for TgCRND8 mice, corresponding to sparse, moderate, and severe Aβ plaque burden, respectively (3). Each brain was separated by hemisphere, where one was flash frozen (FF) and the other formalin-fixed, paraffin-embedded (FFPE) (Figure 2).

Sample and library preparation. Nuclei of FF hemispheres were isolated following the 10x Genomics Demonstrated Protocol (CG000375 Rev B). Paired multiome (Single Cell ATAC [scATAC] and Single Cell Gene Expression) libraries were prepared using the 10x Genomics User Guide (CG000338 Rev D).

For FFPE hemispheres, 5-µm sections were prepared and IF performed following Demonstrated Protocols (CG000408 Rev B and CG000410 Rev B, respectively). Amyloid precursor proteins were immunostained at 1:100 antibody dilutions. Additionally, nuclei were counterstained with DAPI. Imaging was performed on a Nikon Ti2 wide-field fluorescence microscope following Visium for FFPE Imaging Guidelines (CG000436 Rev A). Visium for FFPE libraries were prepared following the User Guide (CG000407 Rev C).

Sequencing. All libraries were sequenced on an Illumina NovaSeq 6000. Multiome libraries were sequenced at a depth of ~20,000 read pairs per cell. Visium for FFPE libraries were sequenced at a depth of ~25,000 read pairs per spot.

Primary data processing. Cell Ranger ARC 2.0 was used to process the multiome assay data, while Space Ranger 1.3 was used to analyze the Visium for FFPE data. After demultiplexing, a separate instance of `cellranger-arc count` was run on each of 12 paired multiome libraries, and `spaceranger count` for each of 12 Visium libraries. The `cellranger-arc aggr` pipeline was used to combine all multiome libraries into a single matrix, while the `spaceranger aggr` pipeline was likewise used to aggregate Visium for FFPE libraries.

Secondary analysis. Quality control was performed using Seurat for gene expression and Visium for FFPE data (4), and Signac for ATAC data (5). Metrics for both assays (number of unique molecular identifiers, number of genes) and percentage of mitochondrial reads were considered to define quality control thresholds.

Dimensionality reduction and visualization. Uniform Manifold Approximation and Projection (UMAP) projections were used for dimensionality reduction and visualization. We used the Weighted Nearest Neighbor (WNN) algorithm to obtain UMAP cell embeddings that consider information from both gene expression and chromatin accessibility assays (6).

Cell-type annotation. Loupe Browser 6.0 was used to perform manual annotation on two multiome and two Visium datasets using a predefined list of 35 marker genes for oligodendrocytes, oligodendrocyte precursor cells, microglia, pericytes/endothelial cells, inhibitory neurons, and astrocytes (Figure 3). An anchor-based algorithm was used to perform automated annotation of spatial and multiome datasets, assigning a probability for each barcode to belong to a specific cell type.

Differential expression. The Wilcoxon test was used to identify differentially expressed genes between transgenic and WT mice in each cell type. A logistic regression was used to quantify differential chromatin accessibility for the multiome data. Peaks and genes were linked using Signac. The differentially accessible regions were used to perform motif enrichment and identify transcription factors with a high probability of binding to those regions.

Anatomical classification and multiomic integration. To deconvolute Visium spots into cell types, we used spacexr in multi-mode, which allows discovery of more than two cell types per spot (7). The aggregated multiome data were used as a reference. Each Visium slide was individually processed to perform cellular deconvolution. Multiomic integration was performed by leveraging trimodal dataset integration in Seurat and assigning cell types to spots and vice versa, while layering on epigenetic information.

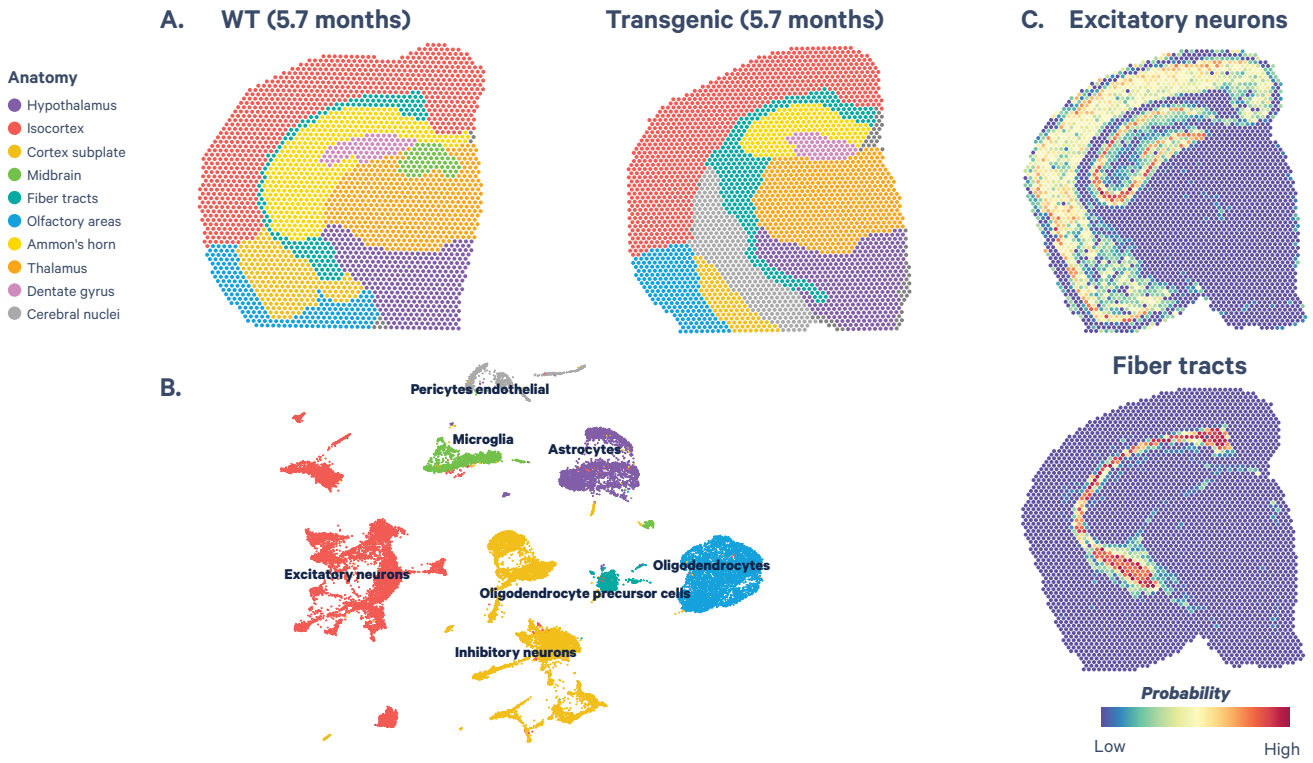

Figure 3. Manual annotation using marker genes. A. Visium sections with anatomical regions manually annotated. **B.** WNN UMAP of manually annotated barcodes. **C.** Results of anchor-based approach to predict anatomical identities and cell-type deconvolution.

Results

Spatial transcriptomics + IF enables localization of plaque-induced gene expression changes

While Visium alone provides a measurement of transcriptome-wide expression in the context of its geographical localization, adding protein detection via IF can identify and localize proteins on the same slide. For example, scientists recently used spatial transcriptomics to reveal multicellular gene co-expression networks in the vicinity of plaque deposits, one of which is a plaque-induced gene (PIG) network mainly involving microglia and astrocytes (2). In the context of AD, Visium with IF enables the identification of gene expression changes in specific cell types that can be associated with nearby features, including intracellular or extracellular inclusions or degenerating neurons, offering a new perspective on disease progression.

Our Visium for FFPE + IF data demonstrated that Aβ plaque burden increases with anatomic specificity over time (Figure 4A), with greater relative abundance in the cortex and dentate gyrus, populated primarily by excitatory neurons, as previously reported. Further analysis of Visium spots showed gene expression patterns dependent on proximity to plaques. Aggregating expression of the PIG set showed gradually decreasing expression from regions at the plaque, toward regions adjacent and distal to it (Figure 4B–D).

Exploring microglia with single cell multiomics

Previous single cell research identified a unique microglial phenotype associated with neurodegenerative diseases (8), which further substantiates these cells as key players in disease pathogenesis and warrants deeper investigation into their precise role.

Solute carriers (SLCs) are a family of transmembrane transporters of nutrients, ions, metabolites, and drugs. Evidence suggests that dysfunction of some SLCs are related to brain disorders, including neurodegenerative diseases (9). We identified *Slc1a3* as differentially expressed in microglia when comparing transgenic and WT mice (Figure 5A). The biggest difference was seen at early timepoints when plaque deposition is sparse.

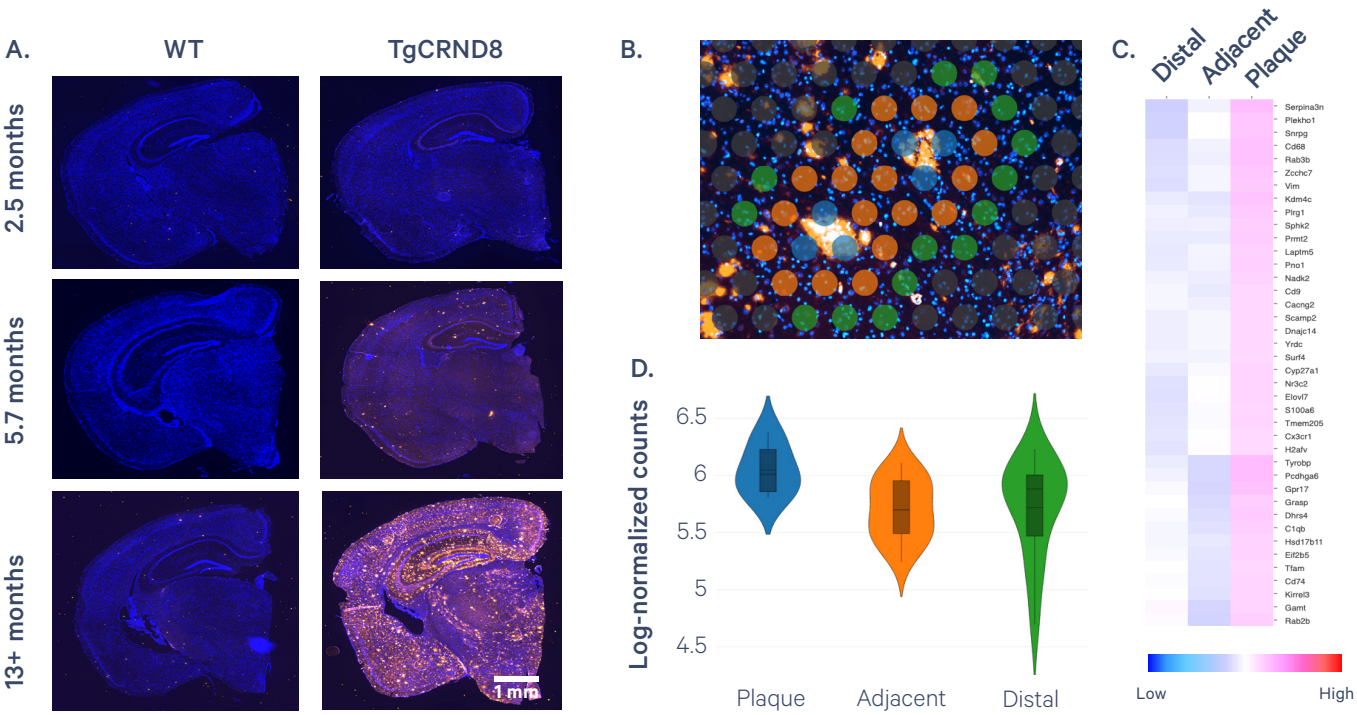

Figure 4. Aβ plaque burden. A. IF assessment of regional plaque burden (blue = DAPI, orange = human amyloid precursor protein). **B.** Close-up of a region within the thalamus of a 13+ month TgCRND8 mouse, with plaque in orange, grouping Visium spots based on the proximity to the plaque as "plaque" (blue), "adjacent" (orange), or "distal" (green). **C.** Heatmap of differentially expressed genes across the three plaque proximity regions. **D.** Violin plots of aggregated expression of the plaque-induced gene (PIG) network.

Using scATAC, we looked for open chromatin regions that showed a strong relationship with gene expression. Paired gene expression and open chromatin signals from the multiome assay pave the way for gene regulatory network predictions by correlating, or linking, open chromatin regions to nearby genes. The nucleotide sequences of these open regions can then be compared against predicted binding motifs to identify transcription factors that may be acting upon that site. In this case, we identified a differentially accessible distal region to *Slc1a3* that may play a role in transcriptional regulation. Motif enrichment highlighted the transcription factors *Egr1, Wt1, Nfyb, Klf4*, and *Znf740* (Figure 5B).

Previous studies have shown that early growth response-1 (EGR1) may play a role in maintaining cholinergic function in the brain in the early stages of AD. In one study, scientists concluded that EGR1 can up-regulate acetylcholinesterase expression, which may contribute cholinergic changes in AD (10). In our Visium for FFPE data, *Egr1* was differentially expressed between transgenic and WT mice. Anatomical annotation of the slides also revealed that the change in expression is primarily localized to the isocortex (Figure 5C–D).

Single cell analysis uncovers oligodendrocyte changes

Oligodendrocytes are the myelinating cells of the central nervous system, and research has increasingly focused on elucidating the role that non-neuronal cells play in AD progression. A recent publication used single cell transcriptomics to evaluate 13 neural cell types, identifying two distinct oligodendrocyte transcriptional states among AD mouse models and noting differences in the effects of AD risk genes on microglia versus non-microglia cells, including oligodendrocytes (11).

Focusing on oligodendrocytes, we observed that *Mon2*, previously found to be differentially expressed in extracellular vesicles from an AD transgenic mouse model (12), was more highly expressed in transgenic mice at the late timepoint when plaque burden is severe (Figure 6A). scATAC analysis showed a weak correlation between gene expression profiles and chromatin accessibility. To perform the motif analysis, we focused on the list of differentially accessible peaks and identified a differentially accessible peak upstream to the transcription start site that could play a regulatory role. Motif enrichment analysis highlighted *Sox8, Rora, Nfya*, and *Sp3* (Figure 6B).

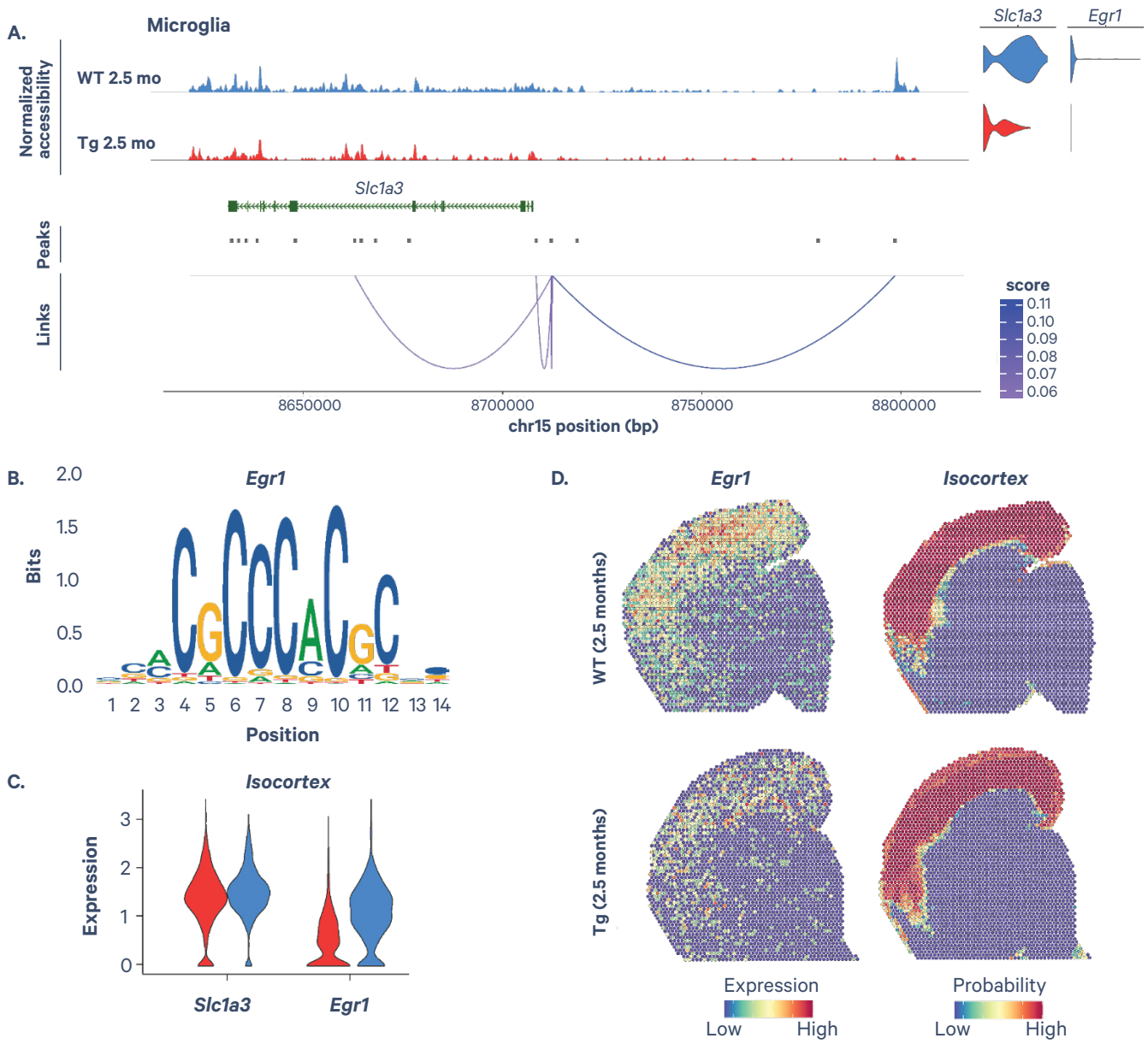

Figure 5. Microglia. Manual annotation using marker genes. A. Chromatin accessibility and expression profiles of regions linked to *Slc1a3* in microglia. **B.** *Egr1* motif enriched in regions upstream to *Slc1a3*. **C.** Violin plot of *Slc1a3* and *Egr1* differential expression in WT (blue) and transgenic (Tg) (red) mice in the isocortex as assessed by Visium for FFPE data. **D.** Spatial expression profile of *Egr1* and Visium spot probabilities belonging to the isocortex region.

It has been previously observed that *Sox8* activation (by notoginsenoside R2, a key saponin in the *Panax notoginseng* plant shown to improve AD symptoms) up-regulates β-catenin expression, helping prevent apoptosis and neuroinflammation in primary rat cortical neurons in an AD setting (13). *Sox8* was among those transcription factors that were found to be enriched using Visium for FFPE. The largest difference was observed in aged mice with advanced plaque burden (13+ months). As expected, anatomical localization of cell-type gene expression signatures revealed oligodendrocytes in the fiber tracts. Differential expression of *Sox8* was detected in overlapping regions, suggesting differential *Sox8* expression is specific to oligodendrocytes (Figure 6C–D).

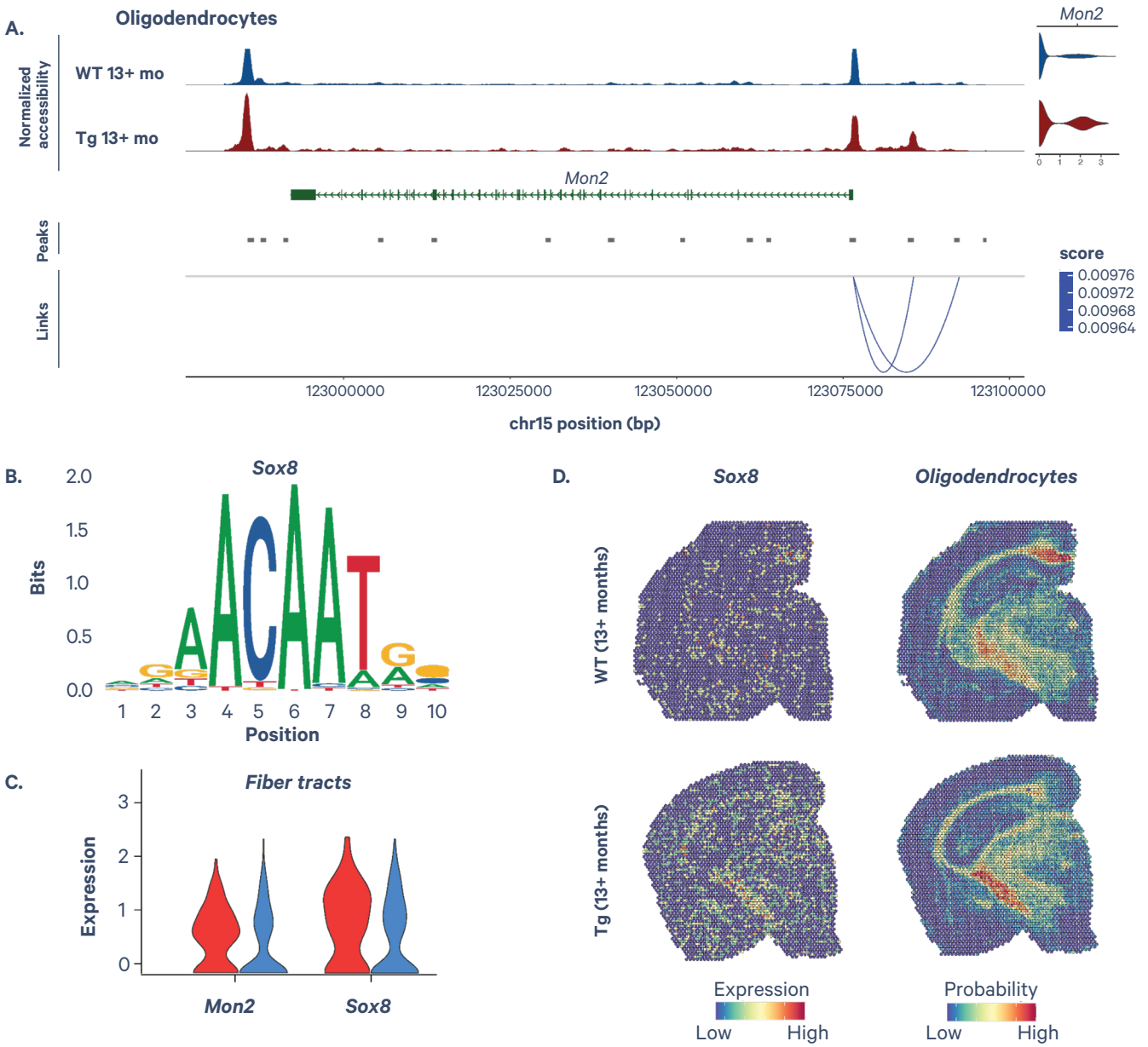

Figure 6. Oligodendrocytes. A. Chromatin accessibility and expression profiles of regions linked to *Mon2* in oligodendrocytes. **B.** *Sox8* motif enriched in regions upstream to *Mon2*. **C.** Violin plot of *Mon2* and *Sox8* differential expression in WT (blue) and Tg (red) mice in fiber tracts as assessed by Visium for FFPE data. **D.** Spatial expression profile of *Sox8* and Visium spot probabilities belonging to oligodendrocytes.

Conclusion

Integrating multiomic single cell gene expression, chromatin accessibility, and spatial transcriptomic data provides a comprehensive approach to detect changes in transcriptional expression and regulation. The data presented in this Application Note demonstrate identification of early- and late-stage markers associated with progressive amyloid deposition, showcasing changes in both gene expression and chromatin accessibility over time in specific cell types and across brain regions in association with neuropathology. Spatial transcriptomics additionally enabled the identification of anatomical regions undergoing significant age-dependent changes in this AD-like mouse model. Together, these data demonstrate the robust nature of a multiomic approach to identify disease markers and reveal dynamic processes occurring over time and across brain regions in association with neuropathology.

References

1. Morabito S, et al. Single-nucleus chromatin accessibility and transcriptomic characterization of Alzheimer's disease. *Nat Genet* 53: 1143–1155 (2021). https://doi.org/10.1038/s41588-021-00894-z
2. Chen W-T, et al. Spatial transcriptomics and in situ sequencing to study Alzheimer's disease. *Cell* 182: 976–991.e19 (2020). https://doi.org/10.1016/j.cell.2020.06.038
3. Chishti MA, et al. Early-onset amyloid deposition and cognitive deficits in transgenic mice expressing a double mutant form of amyloid precursor protein 695. *J Biol Chem* 276: 21562–70 (2001). https://doi.org/10.1074/jbc.M100710200
4. Stuart T, et al. Comprehensive integration of single-cell data. *Cell* 177: 1888–1902.e21 (2019). https://doi.org/10.1016/j.cell.2019.05.031
5. Stuart T, et al. Single-cell chromatin state analysis with Signac. *Nat Methods* 18: 1333–1341 (2021). https://doi.org/10.1038/s41592-021-01282-5
6. Hao Y, et al. Integrated analysis of multimodal single-cell data. *Cell* 184: 3573–3587.e29 (2021). https://doi.org/10.1016/j.cell.2021.04.048
7. Cable D, et al. Robust decomposition of cell type mixtures in spatial transcriptomics. *Nat Biotechnol* 10.1038/s41587-021-00830-w (2021). https://doi.org/10.1038/s41587-021-00830-w
8. Keren-Shaul H, et al. A unique microglia type associated with restricting development of Alzheimer's disease. *Cell* 169: 1276–1290.e17 (2017). https://doi.org/10.1016/j.cell.2017.05.018
9. Chengliang H, et al. The solute carrier transporters and the brain: Physiological and pharmacological implications. *Asian J Pharm Sci* 15: 131–144 (2020). https://doi.org/10.1016/j.ajps.2019.09.002
10. Hu Y-T, et al. Early growth response-1 regulates acetylcholinesterase and its relation with the course of Alzheimer's disease. *Brain Pathol* 29: 502–512 (2019). https://doi.org/10.1111/bpa.12688
11. Lee S-H, et al. TREM2-independent oligodendrocyte, astrocyte, and T cell responses to tau and amyloid pathology in mouse models of Alzheimer's disease. *Cell Rep* 37: 110158 (2021). https://doi.org/10.1016/j.celrep.2021.110158
12. Muraoka S, et al. Enrichment of neurodegenerative microglia signature in brain-derived extracellular vesicles isolated from Alzheimer's disease mouse models. *J Proteome Res* 20: 1733–1743 (2021). https://doi.org/10.1021/acs.jproteome.0c00934
13. Yueqiang H, et al. Notoginsenoside R2 reduces Aβ 25-35-induced neuronal apoptosis and inflammation via miR-27a/SOX8/β-catenin axis. *Hum Exp Toxicol* 40: S347–S358 (2021). https://doi.org/10.1177/09603271211041996

Resources

Explore the multiome and Visium data from these samples further by downloading the following datasets:

Multiome

Visium

Contact us
10xgenomics.com | info@10xgenomics.com